ADVANCED OPTICAL MATERIALS

Supporting Information

for *Adv. Optical Mater.,* DOI: 10.1002/adom.202200458

Directional and Polarized Lasing Action on Pb-free $FASnI_3$ Integrated in Flexible Optical Waveguides

Isaac Suárez, Vladimir S. Chirvony, Jesús Sánchez-Díaz, Rafael S. Sánchez, Iván Mora-Seró,* and Juan P. Martínez-Pastor**

Directional and polarized lasing action on Pb-free $FASnI_3$ integrated in flexible optical waveguides

Isaac Suárez, [1] Vladimir S. Chirvony, [2] Jesus Sanchez-Diaz, [3] Rafael S. Sánchez, [3] Iván Mora-Seró, [3*] and Juan P. Martínez-Pastor [2*]

[1] Escuela Técnica Superior de Ingeniería, Universidad de Valencia, Valencia 46100, Spain.
[2] UMDO, Instituto de Ciencia de los Materiales, Universidad de Valencia, Valencia 46980, Spain.
[3] Institute of Advanced Materials (INAM), Universitat Jaume I, Castelló de la Plana, Castelló 12006, Spain.
*e-mail: isaac.suarez@uv.es, sero@uji.es, juan.mtnez.pastor@uv.es

S1. Basic characterization of $FASnI_3$ thin films.

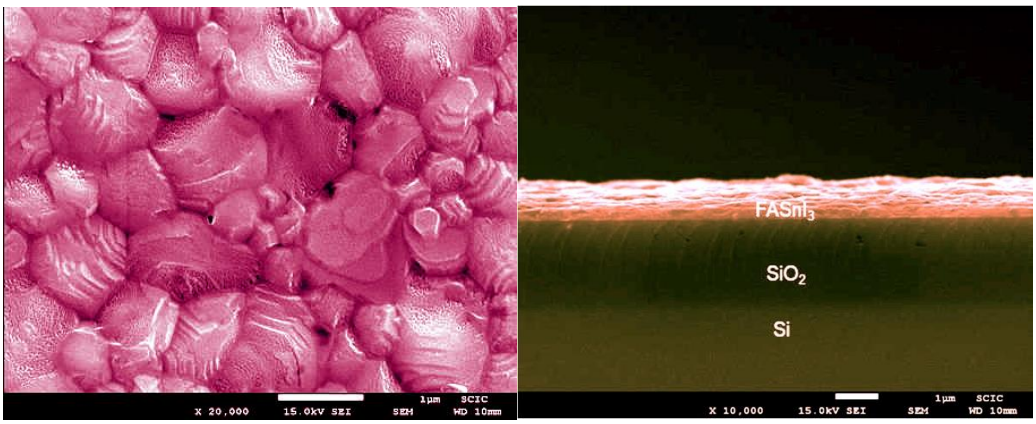

Fig. S1. SEM images of the $FASnI_3$ waveguide deposited onto a SiO_2/Si substrate (left: top view, right: cross section).

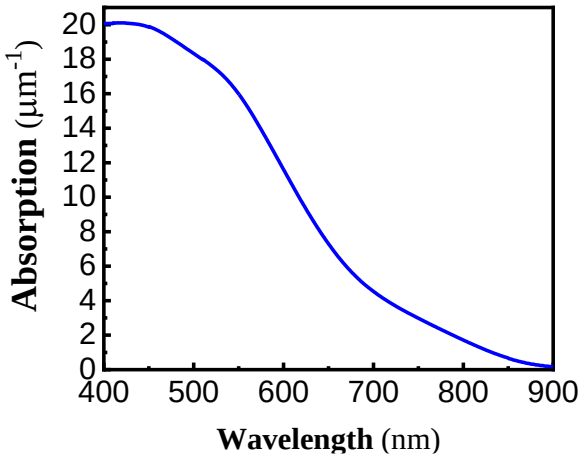

Fig. S2. Absorption of a 200 nm $FASnI_3$ film deposited on a quartz substrate.

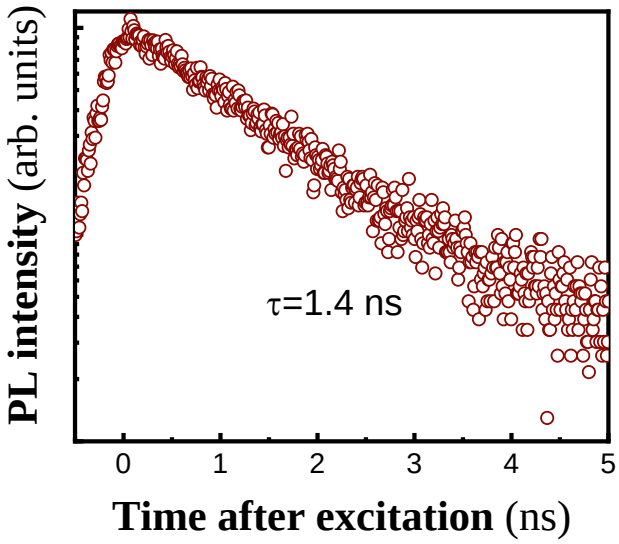

Fig. S3. Time resolved PL of the $FASnI_3$ film deposited on glass excited with 100 fs pulses. A recombination time of around 1.4 ns is deduced.

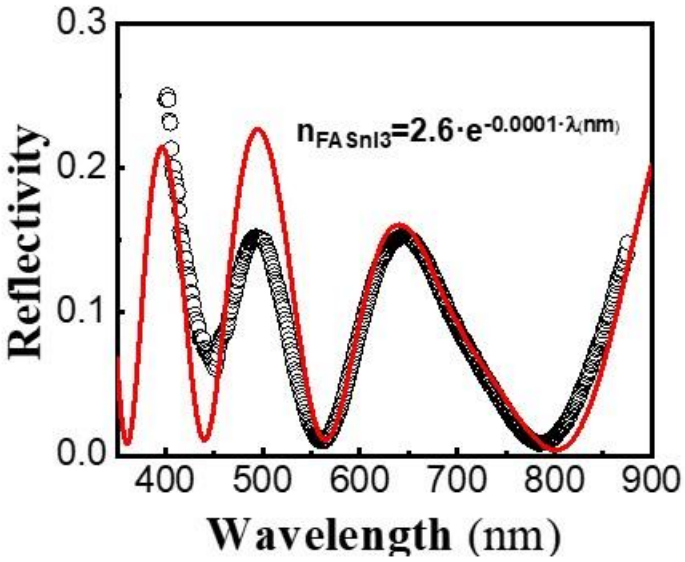

Fig. S4. Reflectivity of a $FASnI_3$ film deposited on a Si substrate. Symbols corresponds to the experimental data and the red solid line to the simulation with the indicated refractive index function.

S2. Propagating modes.

The refractive indices of the materials forming the waveguides are listed in table S1. The structure conforms a planar waveguide whose modes can be calculated with a transfer matrix algorithm. [1] Table S1 presents the effective refractive index of the modes at the pump (532 nm) and PL (890 nm) wavelengths for a waveguide composed by 200 nm and 800 nm thick $FASnI_3$ and PMMA layers, respectively. The refractive indices for Si, SiO_2, and PMMA were obtained from Palik, [2] the refractive index of PET from the results

obtained by Zhang et al., [3] and the refractive index of $FASnI_3$ from the reflectivity measurements (Fig. S3).

Material	532 nm	890 nm
Air	1	1
PMMA	1.492	1.483
FASI	2.4653-0.7231i	2.3786-0.0153i
PET	1.576	1.5531
SiO_2	1.4607	1.4522
Si	4.1353-0.0334i	3.6401-0.0036i

Table S1. Material's refractive indices

The design of the WG is based on the refractive-index contrast (Δn) between the different materials and the engineering of the propagating modes with the geometrical parameters. [4] For this purpose, propagating modes confined in the WG were calculated with a multilayer algorithm in both transverse electric (TE) and transverse magnetic polarization(TM). [1] Table S2 presents the effective refractive indices at 532 nm (pump) and 890 nm (PL) in the rigid (SiO_2/Si) and flexible (PET) substrates. The thickness of the $FASnI_3$ (d_1) is fixed to d_1=200 nm to assure single mode propagation at the PL wavelength (890 nm) in both transverse electric (TE) and transverse magnetic (TM) polarizations. Red line in the inset of Fig. 1 of the manuscript shows the power distribution of the TE_0 mode. This mode is highly confined in the semiconductor with more than 80% of the electric field distribution concentrated in this layer, see red line in the inset of Fig. 1. The TM_0 mode at 890 nm, however, has a smaller effective refractive index, resulting in a lower confinement (62 %) in the active region. On the other hand, the thickness of the PMMA (d_2) is fixed between 600-1000 nm to allow the propagation of the TE_2 (TM_1) cladding mode at the pump wavelength (532 nm), whose power distribution is mainly confined in the polymer (green line). This TE_2 (TM_1) mode is characterization by its lower attenuation, derived from the absence of losses in the PMMA, and the overlap of the evanescent field with the active region (0.2 % of the mode). Then, it represents a suitable mechanism to pump the entire length of the WG (1 mm) by injecting the excitation beam at the input edge of the structure. The introduction of a rigid substrate only results in a slight modification of the propagating modes and their effective refractive indices, see Fig. S5.

Mode	532 nm	890 nm
TE_0	2.27559-0.732i (2.27489-0.734i)	2.05021-0.0138i (2.04207-0.014i)
TE_1	1.6254-0.743i (1.6244-0.757i)	-
TE_2	1.46201-0.0023i (1.46205-0.0022i)	-
TM_0	2.15449-0.737i (2.1512-0.7445i)	1.86211-0.0095i (1.82384-0.0098i)
TM_1	1.45872-0.0083i (1.4580-0.0096i)	-

Table S2. Effective refractive indices of the WG fabricated in PET substrates. In parenthesis the effective refractive index of the WG fabricated on rigid substrates.

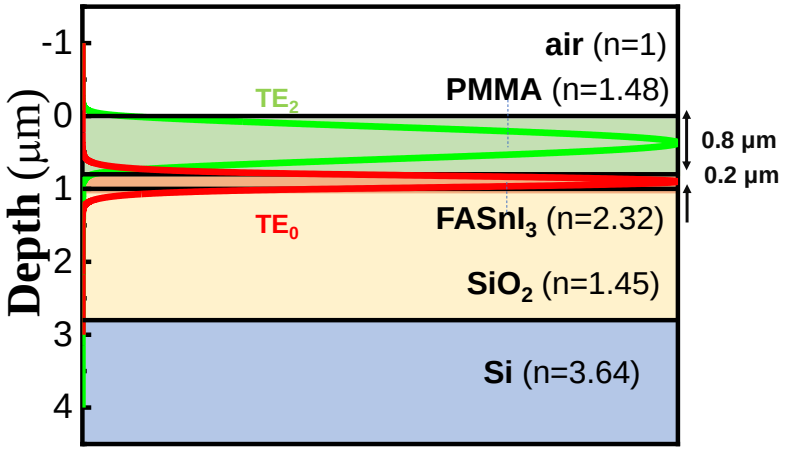

Fig. S5. Propagating modes on a rigid substrate

S3. Nature of lasing.

Compared to a conventional laser, the feedback mechanism of the random lasing (RL) shown in Fig. 2c-d comes from different scattering loops. The origin of this scattering is ascribed here to the grains of the polycrystalline film (see Fig. S1), as previously proposed for $CsSnI_3$ films. [5] Since the scattering efficiency depends on the local sample morphology, the intensity and spectral localization of the narrow spikes vary from sample to sample or between different regions in the same sample. Fig. S6a shows four waveguided spectra exhibiting 2-5 RL lines that were outcoupled at different regions of the rigid WG. The linewidths of RL lines ranged between 1 and 2 meV (0.6-1.2 nm), ten times narrower than the ASE linewidth, which means Q ≈ 700 - 1400. The statistics collected over 200 RL lines indicates that frequencies of the RL peak wavelengths exhibits a distribution consistent with the Lorentzian profile of the ASE spectrum (Fig. S6b). A Fast Fourier Transform (FFT) analysis was performed to measured waveguided ASE spectra containing RL lines to deduce information about the scattering loops, as shown in Fig. S6b. The FFT spectrum of a laser cavity is composed by several Fourier harmonics given by the equation: [7]

$$d_m = \frac{m \cdot L_c \cdot n}{\pi} \quad (2)$$

where d_m is the Fourier harmonics, m is the order of the Fourier harmonic, L_c is the effective optical cavity length, and n is the refractive index of the random lasing material. Each FFT spectrum shows several d_m (see arrows in Fig. S6c) associated to the particular scattering loop or loops during ASE light propagation in the WG. The statistics of the FFT over the 200 measured RL spectra indicates that the harmonics follow approximately two gaussian distribution centered at around d_1=*175 μm* and d_2=*370 μm* (Fig. S6d). Applying equation (2) to these two harmonics, the average cavity lengths would be in the range $L_c \approx$ *231-244 μm*.

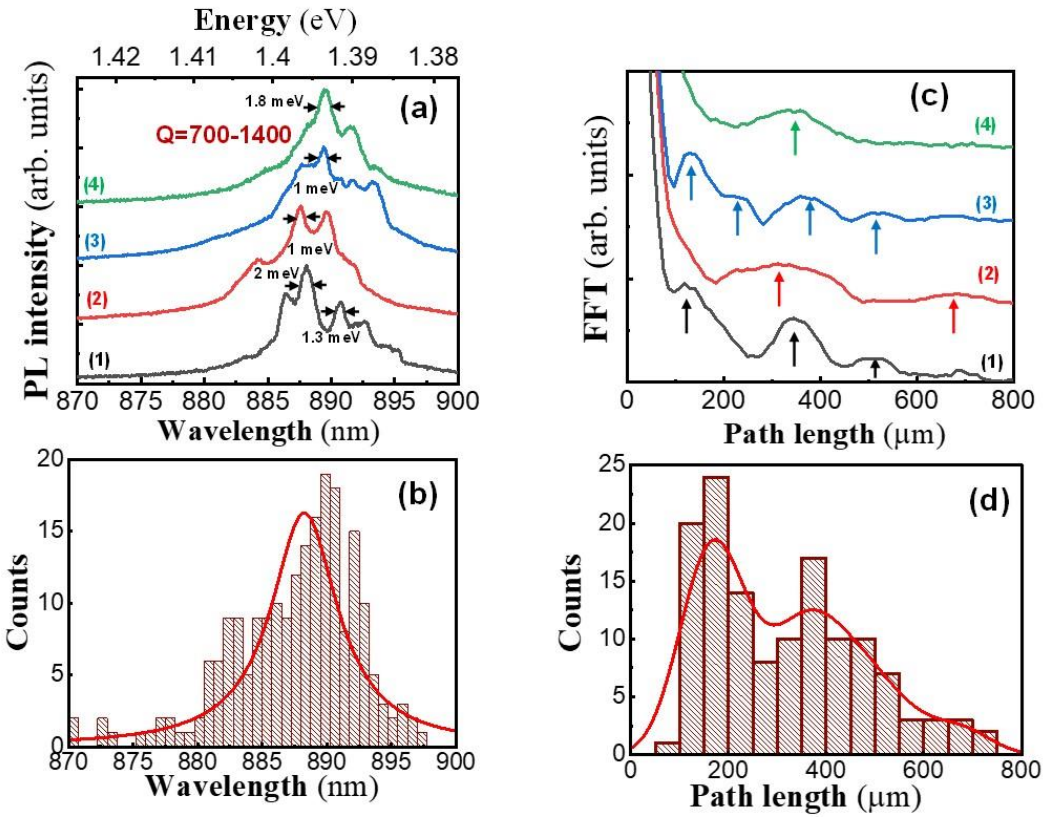

Figure S6. (a) RL emission collected at the output edge of different samples. (b) Statistics of the RL emission over 200 spikes measured in near 100 different excitation points measured in several $FASnI_3$ WG structures. (c) FFT of the RL spectra of Fig. 3(a). The maximum corresponds to each loop size. (d) Statistics of the loop size.

S4. Modelling of lasing generation.

The generation of carriers (n) and photons (S) in our system was fitted by the standard rate equation model for lasers: [11]

$$\frac{\partial n}{\partial t} = G - A_r \cdot n - A_{nr} \cdot n - \Gamma \cdot \sigma \cdot \frac{c}{n_{eff}} \cdot (n - N_0) \quad (1)$$

$$\frac{dS}{dt} = \left(\Gamma \cdot \sigma \cdot \frac{c}{n_{eff}} \cdot (n - N_0) - \frac{1}{\tau_c}\right) \cdot S + A_r \cdot \beta \cdot n \quad (2)$$

where A_r is the radiative recombination rate (inverse of the recombination time), A_{nr} is the nonradiative recombination rate, σ the gain cross section, N_0 the transparence carrier density, n_{eff} the effective refractive index of the TE_0 mode at 890 nm, Γ the confinement of the TE_0 mode at 890 nm in the FASI film, S the photon density, c the speed of light, τ_c the accounts the loss of photons inside waveguide/cavity,), β the spontaneous emission factor, R a factor related with the generation of spontaneous emission inside the waveguide, and G is the photogeneration of electron-hole pairs:

$$G = \frac{P}{A \cdot h\nu} \cdot \alpha_p \quad (3)$$

where *P(z)* is the excitation peak power overlapping the active region, α the absorption coefficient at the excitation wavelength, *A* the area of excitation and $h\nu$ the energy of the pump photon at 532 nm (2.33 eV). Equations (1-2) have included the optical gain in the system that is given by:

$$g = \Gamma \cdot \sigma \cdot (n - N_0) \quad (4)$$

Equations (1-4) nicely fit the experimental results of the PL shown in the Fig. 2 of the manuscript with α_p=17.08 μm^{-1}, A_r= 0.7 ns^{-1}, A_{nr}=0, Γ=0.8, n_{eff}=2.05, σ= 1 ·10^{-14} cm^2 N_0=2·10^{17} cm^{-3}, τ_c=3 *ps* and β=0.7. Here Γ and n_{eff} were obtained from the mode analysis (section S2); α_p (Fig. S2), A_r (Fig. S3), and N_0 from our experimental data; A_{nr} is neglected; σ from the condition that g=-α_s when n=0, where α_s is the losses of the TE_0 mode at 890 nm; and τ_c, β from the best fitting parameters.

S5. Recombination time in flexible substrate.

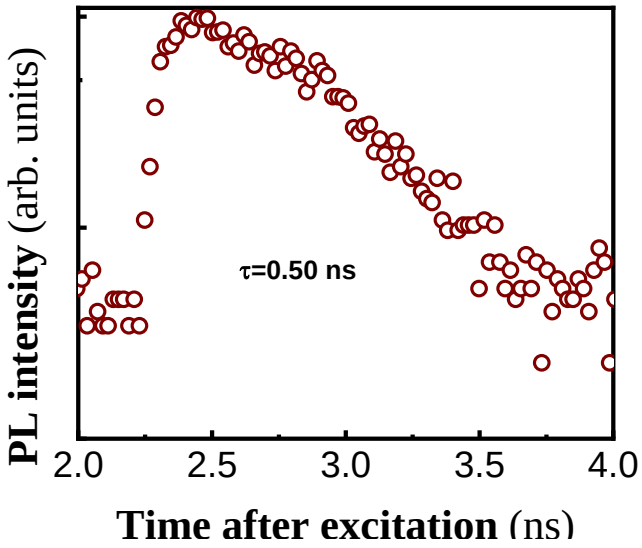

Fig. S7. Time resolved PL of the $FASnI_3$ film deposited on glass excited with 100 fs pulses. A recombination time of around 1.4 ns is deduced.

S6. Evolution of RL with time on a flexible substrate.

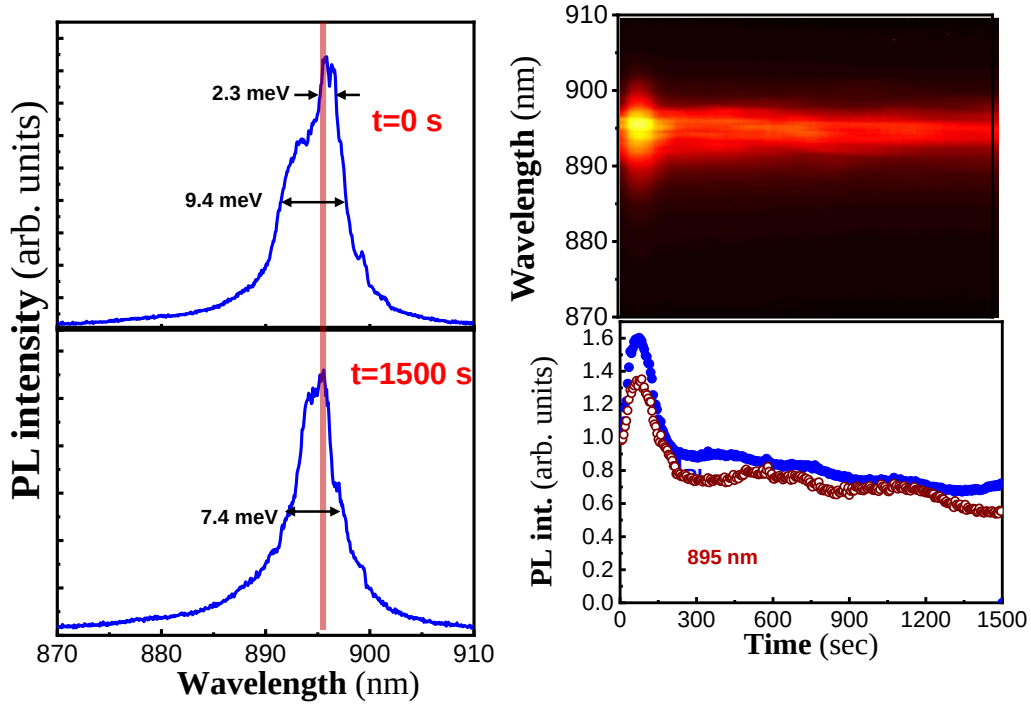

Fig. S8. Evolution of the RL action during the time in a flexible substrate. (a) Spectra at t=0. (b) Spectra at t=1500 s. (c) MAP of the PL spectra as a function of the time. (d) Evolution of the integrated PL intensity (I_{PL}) and RL lines at 888 nm (green symbols) and 892 nm (brown symbols).

S6. Random Laser spectra measured by back-scattering geometry.

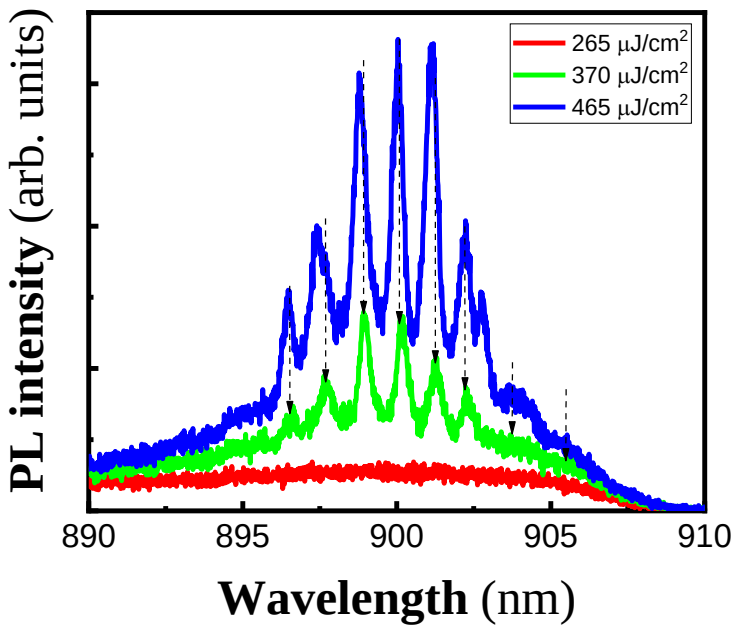

Fig. S9. RL spectra measured under back-scattering geometry.

S8. Polarization on a flexible substrate.

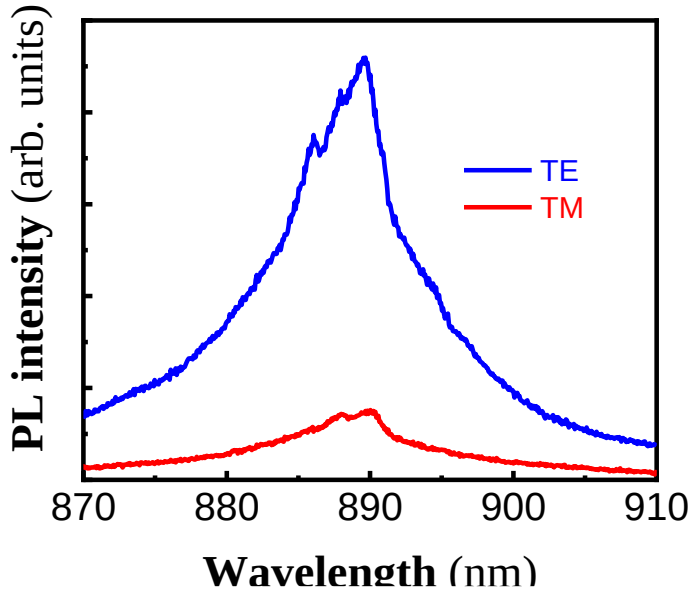

Fig. S10. PL decoupled at the output edge of the PET flexible substrate in TE (blue) and TM (red) polarization. There is a strong polarization dependence for the outcoupled light of the flexible WG with 86 % of the total PL intensity in TE.

S9. Bending of the flexible substrate.

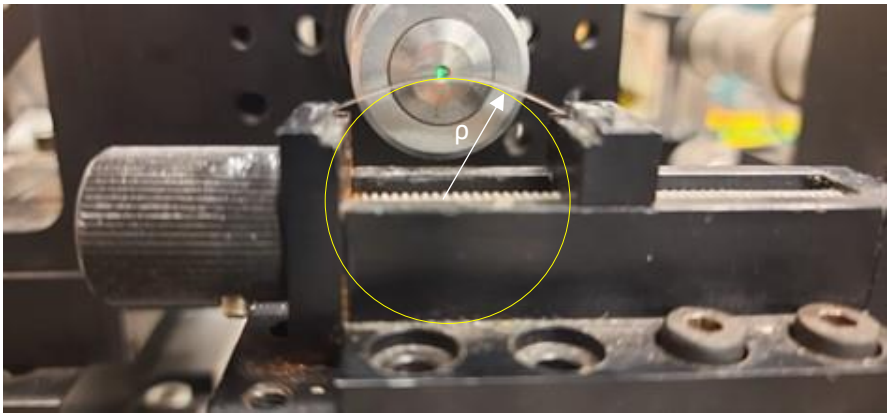

Fig. S11. Photograph of the sample under bending conditions. The curvature radius (ρ) is calculated as the radius of the circumference tangential to the output edge of the waveguide.

S10. Characterization before and after bending.

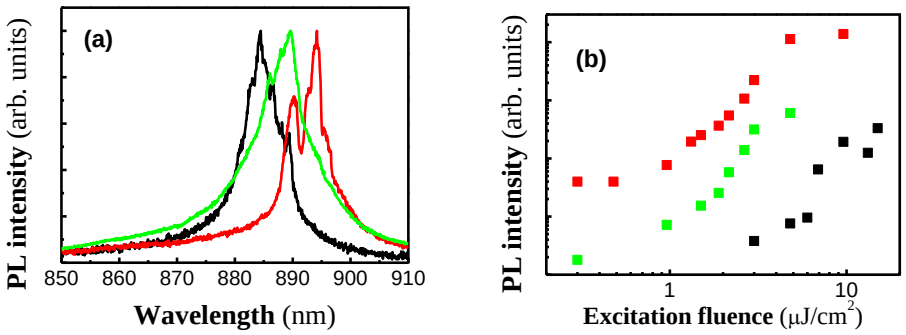

Fig. S12. PL spectrum and log-log plot before bending (black), after bending (red), measurement in another sample (green). The different intensities and peak ASE wavelengths are attributed to different coupling efficiencies, waveguide lengths or RL paths.